The permeability transition in human mitochondria persists in the absence of peripheral stalk subunits of ATP synthase

Jiuya He, Joe Carroll, Shujing Ding, Ian M. Fearnley and John E. Walker

Medical Research Council Mitochondrial Biology Unit, University of Cambridge, Cambridge Biomedical Campus, Hills Road, Cambridge CB2 0XY, United Kingdom

*To whom correspondence should be addressed. J. E. W., Tel.: +44-1223-252701; e-mail: walker@mrc-mbu.cam.ac.uk

Running title: The mitochondrial permeability transition pore

The authors declare no conflict of interest

Author contributions: J. E. W. designed research and supervised project; J. H., J. C., S. D. and I. M. F. performed research; J. H., J. C., S. D., I. M. F. and J. E. W. analysed data, and J. E. W. prepared the manuscript.

Classification: BIOLOGICAL SCIENCES, Biochemistry

Key words: human mitochondria; ATP synthase; permeability transition pore; subunit b; oligomycin sensitivity conferral protein; *ATP5F1*; *ATP5O*

Significance

Mitochondria generate the cellular fuel, adenosine triphosphate, or ATP, to sustain complex life. Production of ATP depends on the oxidation of energy rich compounds to produce a chemical potential difference for hydrogen ions, the proton motive force (pmf), across the inner mitochondrial membrane (IMM). Disruption of the IMM, dissipation of the pmf and cell death occur if the concentration of calcium ions inside mitochondria is elevated sufficiently to open a pore in the IMM. The identity of the pore is disputed. One proposal is that the pore is in the enzyme that makes ATP. Here, we show that proteins in the enzyme's peripheral stalk are not involved in the formation or regulation of the pore. (115 words)

Abstract

The opening of a non-specific channel, known as the permeability transition pore (PTP), in the inner membranes of mitochondria, can be triggered by calcium ions, leading to swelling of the organelle, disruption of the inner membrane and ATP synthesis, and cell death. Pore opening can be inhibited by cyclosporin A mediated via cyclophilin D. It has been proposed that the pore is associated with the dimeric ATP synthase, and that the OSCP (oligomycin sensitivity conferral protein), a component of the enzyme's peripheral stalk, provides the site where cyclophilin D interacts. Subunit b contributes a central α-helical structure to the peripheral stalk, extending from near the top of the enzyme's catalytic domain and crossing the membrane domain of the enzyme via two α-helices. We investigated the possible involvement of the subunit b and the OSCP in the PTP by generating clonal cells, HAP1-Δb and HAP1-ΔOSCP, lacking the membrane domain of subunit b or the OSCP, respectively, in which the correponding genes *ATP5F1* and *ATP5O* had been disrupted. Both cell lines preserve the characteristic properties of the PTP. Therefore, the membrane domain of subunit b does not contribute to the PTP, and the OSCP does not provide the site of interaction with cyclophilin

D. The membrane subunits ATP6, ATP8 and subunit c have been eliminated previously from possible participation in the PTP. Therefore, the only subunits of ATP synthase that could participate in pore formation are e, f, g, DAPIT (diabetes associated protein in insulin sensitive tissues) and the 6.8 kDa proteolipid. (250 words).

Introduction

In 1976, Hunter, Haworth and Southard (1) demonstrated that bovine heart mitochondria respond to the elevation of the concentration of exogenous Ca^{2+} ions to high levels by opening a non-specific channel, now known as the mitochondrial permeability transition pore (PTP). In consequence, the mitochondria took up water, their cristae became swollen and their membranes were disrupted. Since then, these observations have been replicated in mitochondria *in situ* in many cell types, and, in addition to elevated Ca^{2+} ion concentration, other effectors of opening of the PTP have been identified, including phosphate, adenine nucleotide depletion, and thiol oxidants (2). Today, it is well established that the opening of the PTP disrupts ion homeostasis and the synthesis of ATP, and the mitochondrial membranes lose their integrity, leading to cell-death (3). The PTP in isolated mitochondria can be opened experimentally by the introduction of thapsigargin (4), an inhibitor of the Ca^{2+}-ATPase in the sarcoplasmic and endoplasmic reticula, at high non-specific concentrations. In cultured human cells the PTP can be opened by providing a route for ingress of exogenous Ca^{2+} ions by permeablizing the plasma membrane either with ionophores such as ferutinin (5), or with the mild detergent digitonin (6). The cytoplasmic Ca^{2+} ions are taken up into the mitochondrial matrix by the Ca^{2+}-uniporter (7, 8), a component of the inner membrane, and when the total concentration of Ca^{2+} ions in the mitochondrial matrix is sufficiently elevated, the PTP opens. A characteristic feature of the PTP is that its opening can be inhibited by cyclosporin A (9) via the binding of the drug to cyclophilin D (10–13). Cyclophilin D is a

prolyl cis-trans isomerase found in the mitochondrial matrix, and it is considered to interact with and modulate the PTP rather than being an integral component (14).

The opening of the PTP and the associated effects have been linked to human diseases including cardiac ischemia, neurodegeneration, cancer and muscle dystrophy, and thus knowledge of the proteins that form the PTP has considerable medical relevance (15). Several proposals have been made about possible protein constituents of the PTP including the ADP/ATP translocase, which is the predominant transport protein in the inner membranes of mitochondria, and the voltage dependent anion channel found in the outer membrane of the organelle, but neither of these proposals has withstood scrutiny (16, 17). A further proposition, that another component of the inner mitochondrial membrane, the AAA-protease, SPG7, participates in formation of the PTP, has been disputed (18, 19) (AAA is ATPase associated with diverse cellular activities, and SPG7, paraplegin matrix AAA-peptidase subunit). Yet another proposition, investigated here, is that the PTP is associated with the dimeric ATP synthase complex (20), another abundant constituent of the inner mitochondrial membrane. Each monomer of the dimeric mammalian complex is an assembly of 28 proteins of 18 different types organised into two domains (Fig. 1). The F_1-catalytic domain sits above the membrane domain, and the two domains are linked by the central stalk (subunits γ, δ and ε), and by the peripheral stalk (subunits OSCP, or oligomycin sensitivity conferral protein, b, d and F_6) (21). The OSCP has been proposed to provide the site of interaction of the PTP with cyclophilin D (20).

If the PTP is associated with the ATP synthase complex, it seems likely that it will involve one or more of the membrane subunits of the enzyme. One specific proposal, that the PTP is provided by a ring of eight c-subunits in the membrane sector of the enzyme's rotor (22, 23) has been disproved in a clonal cell line where the three genes encoding the c-subunit have

been disrupted (24). Although these cells are incapable of making the c-subunit, the characteristic properties of the PTP persist (24). Another possibility that two other membrane components of the ATP synthase, subunits a (or ATP6) and A6L (or ATP8) might participate in the formation of the PTP has been disproved also; in human ρ^o-cells, which lack the mitochondrial genome, and therefore are devoid of both subunits, the PTP persists (24, 25).

Here, we have tested the possible participation of the b-subunit in the PTP. This subunit has two transmembrane α-helices that help to hold the a-subunit against the c-ring (Fig. 1) (26–28). The remainder of the protein is folded into a single α-helix 150 Å long, extending away from the inner membrane towards the $\alpha_3\beta_3$-domain, and providing the core of the peripheral stalk (29, 30). The associated d- and F_6-subunits are largely α-helical also, and form a bundle of parallel α-helices with the b-subunit (26–30). We have disrupted the corresponding gene, *ATP5F1*, in a near haploid cell line, and studied whether removal of the b-subunit affects the functioning of the PTP. In addition, we have investigated whether the OSCP provides the site of binding for cyclophilin D. The OSCP is located at the upper end of the peripheral stalk in Fig. 1, and has two domains. The N-terminal α-helical domain is joined to the $\alpha_3\beta_3$-domain via interactions with the N-terminal regions of the three α-subunits, and the C-terminal domain connects the OSCP with the C-terminal region of the b-subunit (26–28, 30). In experiments described below, we have disrupted *ATP5O*, the gene that encodes the OSCP, and we have examined the effect of removing the OSCP on the susceptibility to inhibition of the opening of the PTP by cyclosporin A mediated via cyclophilin D.

Results

Human Cells Devoid of Subunit b and the OSCP. HAP1 cells have a haploid karyotype, but a fragment of chromosome 15 is located in chromosome 19, and there is a reciprocal translocation between chromosomes 9 and 22 (31, 32). Neither of these features affects

ATP5F1 and *ATP5O* encoding subunit b and the OSCP, respectively, as *ATP5F1* gene is on chromosome 1 and *AT5PO* is on chromosome 21. Pairs of guide RNA molecules characteristic of exons I and introns A in *ATP5F1* and *ATP5O* genes were selected (see Fig. S1 and Table S1). Each pair was introduced independently into HAP1-WT (wild-type) cells, and clones arising from single cells, identified as having expressed Cas9, were screened for the absence of either subunit b or the OSCP. In this way, HAP1-Δb and HAP1-ΔOSCP cells, lacking subunit b or the OSCP, respectively, were identified (Fig. 2). Analysis of the DNA sequences in the regions of the human genome where *ATP5F1* is found in HAP1-Δb, and *ATP5O* in HAP1-ΔOSCP (Table S2 and Fig. S1), showed that 62 and 214 base pairs had been deleted, respectively. In addition, a single base had been inserted at the deletion site in *ATP5O*. Each deletion had arisen from two gRNAs and non-homologous end-joining of the deleted genomic DNA. Human cells encode a precursor of the b-subunit where the mature protein is preceded by a mitochondrial import sequence of 42 residues (33). The deletion in *ATP5F1* removed the translational initiator codon of the precursor, 20 bases upstream, codons 2-13 plus the first base of codon 14, and extended 2 bases into intron A. The OSCP has an N-terminal mitochondrial import sequence of 23 amino acids (34), and the deletion in *ATP5O* also removed the translational initiator codon plus 88 bases upstream, and codons 2-12, and extended 90 bases into intron A.

Characteristics of HAP1-Δb and HAP1-ΔOSCP Cells. The HAP1-Δb and HAP1-ΔOSCP cells grew more slowly than the HAP1-WT cells (Fig. S2A), and the copy number of mitochondrial DNA was reduced by 8% in the former and by 30% in the latter (Fig. S2B). Relative to HAP1-WT cells, the levels of complexes I, III and IV, but not of complex II, were reduced in both derivative cell lines (Fig. S2C), and hence they have a lower respiratory capacity (Fig. S2D and S2E).

Pore Opening in HAP1-Δb and HAP1-ΔOSCP Cells. Under the optimum conditions established before (24), the opening of the PTP in intact HAP1-WT cells was demonstrated in the presence of both thapsigargin and the calcium ionophore ferutinin, and with both reagents, opening of the PTP was prevented by addition of cyclosporin A. Similar results were obtained with HAP1-Δb and HAP1-ΔOSCP cells (Fig. 3). Other experiments on PTP opening were conducted with HAP1-WT, HAP1-Δb and HAP1-ΔOSCP cells where their plasma membranes had been permeabilized with digitonin. In one set of experiments, the responses of the cells to successive pulses of Ca^{2+} were monitored with Calcium-green-5N in the absence and presence of cyclosporin A (Fig. 4, and Tables S3, S4 and S5). On average, the ratios of the number of calcium pulses required to induce the PTP in the presence and absence of cyclosporin A were similar; the values were 2.63±0.48 (n=8) in HAP1-WT cells, 2.48±0.42 (n=4) in HAP1-Δb cells, and 2.22±0.36 (n=6) in HAP1-ΔOSCP cells. Thus, in response to pulses of exogenous Ca^{2+}, there was no significant difference in PTP opening in the presence and in the absence of either subunit b or the OSCP. As expected, in HAP1-WT and HAP1-Δb cells, inhibition of the mitochondrial calcium uniporter with Ru360 immediately after a single calcium injection prevented any further uptake of Ca^{2+} by mitochondria (Fig. S3). In a second set of experiments with HAP1-WT, HAP1-Δb and HAP1-ΔOSCP cells, with their plasma membranes permeablized with digitonin, the decrease in absorbance at 540 nm following the addition of exogenous Ca^{2+}, was consistent with the opening of the PTP and the swelling of the mitochondria in all three cell types. In each case, in the presence of cyclosporin A, the addition of exogenous Ca^{2+} was not accompanied by a decrease in absorption at 540 nm (Fig. 5).

The Vestigial ATP Synthase Complexes in HAP1-Δb and HAP1-ΔOSCP Cells. Despite the significant effect of the removal of either subunit b or the OSCP on cellular respiration, the mitochondria of both HAP1-Δb and HAP1-ΔOSCP cells still retain an assembled vestigial

ATP synthase complex. Analysis of this complex by SDS-PAGE analysis and mass spectrometric analysis of the bands showed that it contained a complete complement of the subunits that form the F_1-catalytic domain (subunits α, β γ, δ and ε) plus subunit c; these are the components of the F_1-c_8 ring subcomplex (Fig. 6A). In HAP1-ΔOSCP cells, an elevated amount of one mature form of IF_1, IF_1-M1, was associated with the complex. Examination of the vestigial complexes by quantitative mass spectrometry confirmed their subunit compositions (Figs. 6B, 6C and S4; Datasets S1 and S2). Also detected were elevated levels of mature IF_1 in the complex from both HAP1-Δb and HAP1-ΔOSCP cells, and of the import precursor of IF_1, IF_1-P in the complex from HAP1-ΔOSCP cells. There was a small amount of OSCP in the complex from HAP1-Δb cells, but peripheral stalk subunits d and F_6, supernumerary subunits e, f, g, DAPIT and 6.8PL and the mitochondrial encoded subunits ATP6 and ATP8 were not detected at significant levels. Relative to the levels of intact ATP synthase present in HAP1-WT cells, the level of the vestigial complex was reduced to approximately 30% in HAP1-Δb cells and 65% in HAP1-ΔOSCP cells. The quantitative analysis of samples of mitoplasts from HAP1-Δb and HAP1-ΔOSCP cells (Figs. S4 and S5; Datasets S3 and S4) confirmed the findings with the purified vestigial complexes, but also in the mitoplasts from both cells, significant but low levels of peripheral stalk subunits (F_6 and OSCP in HAP1-Δb, and F_6 in HAP1-ΔOSCP cells) remain. In addition, supernumerary subunits (e, f, g, DAPIT and 6.8PL) and ATP8 were present at low levels in HAP1-ΔOSCP cells.

The most surprising aspect of these quantitative mass spectrometry analyses was that they provided evidence for the presence at low levels (0.6%, based on peptide intensities) in the HAP1-Δb cells of five tryptic peptides representing residues 74-89, 90-97, 98-112, 122-129 and 130-141 of the membrane extrinsic region of the mature b-subunit. These peptides are

derived from a region of the SDS-PAGE gel corresponding to a truncated b-subunit (apparent molecular weight 17.5 kDa). However, there was no evidence for peptides originating from the N-terminal region of the b-protein. In order to understand the origin of these peptides, RNA transcripts covering the region that could code for these peptides in HAP1-Δb cells were amplified by PCR and sequenced. These analyses showed that transcription had occurred in HAP1-Δb cells by use of an alternative splice site in intron A (see Fig. S6), allowing translation to begin from the ATG codon encoding methionine-67 in the wild-type b-subunit, thereby producing a truncated b-subunit (residues 67-214) lacking the membrane intrinsic region of the mature b-subunit. There was no evidence in the quantitative mass spectrometry experiments for production of a truncated OSCP subunit by a similar mechanism.

Oligomeric State of Vestigial ATP Synthases. The PTP has been proposed to be associated with dimers, and not monomers of the ATP synthase complex. Therefore, the oligomeric state(s) of the vestigial complexes in HAP1-Δb and HAP1-ΔOSCP cells, which are identical in their subunit compositions, were investigated by native gel electrophoresis of digitonin extracts of mitoplasts (Fig. 7). These analyses, made at several concentrations of digitonin, showed that the vestigial ATP synthase complexes from both HAP1-Δb and HAP1-ΔOSCP cells, ran to a position on the gels corresponding to a monomeric F_1-c_8 sub-complex of ATP synthase (Fig. 7A). There was no evidence for a dimeric form of the sub-complex. Moreover, when the gels were probed with antibodies against supernumerary subunit g (Fig. 7B) and peripheral stalk subunits d and F_6, there was no evidence for any separate sub-complex containing these subunits.

Discussion

The experiments described above with HAP1-Δb and HAP1-ΔOSCP cells demonstrate conclusively by four independent assays of the PTP that, even when the membrane region of

the b-subunit or the entire OSCP subunit is absent from their mitochondria, the cells retain a functional PTP. In intact HAP1-Δb and HAP1-ΔOSCP cells, the PTP opens characteristically in response to treatment with either thapsigargin or ferutinin (Fig. 3). Likewise, in permeabilized HAP1-Δb and HAP1-ΔOSCP cells, the PTP opens in response to several pulses of extramitochondrial Ca^{2+}, and a single bolus of 200 μM calcium chloride causes the mitochondria in the permeabilized cells to swell (Figs. 4 and 5). In all of these assays, opening of the PTP could be inhibited by cyclosporin A. Therefore, the two transmembrane α-helices of subunit b are not an essential component of the PTP, as the pore remains functional in their absence. Moreover, the OSCP does not provide the site of interaction of cyclophilin D with the PTP, as the opening of the pore remains sensitive to inhibition by cyclosporin A in the absence of the OSCP.

The mitochondria of both HAP1-Δb and HAP1-ΔOSCP cells contain a vestigial ATPase complex with the subunit composition of the F_1-domain plus the c-subunit, presumably representing the F_1-c_8 component of the intact ATP synthase. The closely related F_1-c_8 complex from bovine mitochondria has been isolated and characterized (35). It is capable of hydrolyzing ATP, but it is unable to carry out the synthetic reaction. However, the human vestigial complexes in HAP1-Δb and HAP1-ΔOSCP cells are associated with IF_1-M1, one of two observed mature forms of IF_1, where residues 1-24 have been removed from the mitochondrial import precursor, IF_1-P (24). The mature inhibitor protein acts by forming a 1:1 inhibited complex with F_1-ATPase (36). The relative molar quantities of IF_1-M1 and the vestigial complex have not been measured in either HAP1-Δb and HAP1-ΔOSCP cells, but it is reasonable to assume that at least some of the hydrolytic activity of the vestigial complexes will be inhibited by this protein. In addition, in HAP1-ΔOSCP cells, IF_1-P itself is also associated with the vestigial complex (Fig. 6). Previously, this mitochondrial import precursor

protein has been observed intact in association with another related but distinct vestigial ATPase complex inside the mitochondria derived from human ρ^0-cells (24, 37). It is not known whether IF_1-P follows the same pathway of entry into the mitochondria of these cells as IF_1-M1, or whether indeed IF_1-P is capable of inhibiting ATP hydrolysis. In the bovine inhibited complex, the inhibitory region of mature IF_1 from residues 21-50 forms an α-helix that occupies a deep groove in the catalytic interface between the α_{DP}- and β_{DP}-subunits; residues 14-18 interact with the coiled-coil region of the γ-subunit via a short α-helix; residues 8-13 form an extended structure; residues 1-7 are disordered and they extend into the central aqueous cavity of F_1-ATPase (38, 39). The mode of binding of IF_1-P to the sub-complex is not known, but it seems possible that the presence in IF_1-P of the additional twenty-four N-terminal residues might impede binding of the protein to the site occupied by mature IF_1 in the inhibited complex.

The removal of either subunit b or the OSCP destabilises the peripheral stalk, and none of its four constituent subunits (OSCP, b, F_6, and d) nor the associated ATP8 subunit, is present in the vestigial sub-complex from HAP1-ΔOSCP cells, and also in HAP1-Δb, except that traces of the OSCP were detected. In the absence of the peripheral stalk and ATP8, ATP6 no longer has any support to maintain it in contact with the c_8-ring (26–28). Therefore, ATP6, and the supernumerary subunits (e, f, g, DAPIT and 6.8PL) associated with ATP6 and the membrane domain of subunit b, are also absent from the sub-complex (Fig. 6). As depicted in Fig. 1, subunit f is probably associated with subunits ATP6 and ATP8 (27), and in the dimeric complex, subunits e and g probably form the interface between monomers, with subunits DAPIT and 6.8PL together in a more peripheral position, relative to the dimer interface. Clearly, this dimer interface is not present in the vestigial complexes from HAP1-Δb and HAP1-ΔOSCP cells. However, subunits e, f and g (and other supernumerary subunits) are still present in the mitoplasts of HAP1-Δb and HAP1-ΔOSCP cells, albeit at reduced levels relative

to HAP1-WT cells (Fig. S5). In native gels of digitonin extracts of mitoplasts (Fig. 7), although there was no evidence for a separate sub-complex, monomeric or dimeric, involving subunit g, it remains possible that such a sub-complex was present in the mitoplast membranes, and that it was disrupted by the conditions of extraction with digitonin. As noted before, dimers of the integral dimeric ATP synthase itself can become disrupted artefactually by this process (24, 40). Therefore, in order to eliminate any possibility of the participation of subunits e and g (and subunits f, DAPIT and 6.8PL) in forming the PTP, it will be necessary to remove each of them by gene disruption experiments and to examine the consequences of doing so.

Materials and Methods

Human HAP1 and mutant cells derived from them were grown under standard conditions. Oxygen consumption rates were measured in a Seahorse XF24 instrument. A*TP5F1* and *ATP5O* were disrupted in HAP1 cells by CRISPR-Cas9 technology (41). ATP synthase and sub-complexes of it were purified from mitoplasts by immuno-capture. Proteins were subject to stable isotope labelling in cell culture (SILAC). Labelled proteins were quantitated by mass spectrometry. Opening of the PTP was assayed by four methods. In intact HAP1 cells, pore opening was induced by thapsigargin (4), or ferutinin (5), and, in HAP1 cells where the plasma membrane had been permeabilized with digitonin, by examination of the capacity of the mitochondria to retain Ca^{2+} introduced exogenously (42), and by monitoring the swelling of mitochondria in response to a pulse of 200 μM calcium chloride (43) in the absence and presence of cyclosporin A.

For full details of these processes, see Supplementary Information.

Acknowledgements. This work was supported by the Medical Research Council, UK by Programme grant [MR/M009858/1] to J. E. W.

References

1. Hunter DR, Haworth RA, Southard JH (1976) Relationship between configuration, function, and permeability in calcium-treated mitochondria. *J Biol Chem* 251(16):5069–5077.
2. Zoratti M, Szabò I (1995) The mitochondrial permeability transition. *Biochim Biophys Acta* 1241(2):139–176.
3. Kwong JQ, Molkentin JD (2015) Physiological and pathological roles of the mitochondrial permeability transition pore in the heart. *Cell Metab* 21(2):206–214.
4. Korge P, Weiss JN (1999) Thapsigargin directly induces the mitochondrial permeability transition. *Eur J Biochem* 265(1):273–280.
5. Abramov AY, Duchen MR (2003) Actions of ionomycin, 4-BrA23187 and a novel electrogenic Ca^{2+} ionophore on mitochondria in intact cells. *Cell Calcium* 33(2):101–112.
6. Chauvin C *et al.* (2001) Rotenone inhibits the mitochondrial permeability transition-induced cell death in U937 and KB cells. *J Biol Chem* 276(44):41394–41398.
7. De Stefani D, Raffaello A, Teardo E, Szabò I, Rizzuto R (2011) A forty-kilodalton protein of the inner membrane is the mitochondrial calcium uniporter. *Nature* 476(7360):336–340.
8. Baughman JM *et al.* (2011) Integrative genomics identifies MCU as an essential component of the mitochondrial calcium uniporter. *Nature* 476(7360):341–345.
9. Crompton M, Ellinger H, Costi A (1988) Inhibition by cyclosporin A of a Ca^{2+}-dependent pore in heart mitochondria activated by inorganic phosphate and oxidative stress. *Biochem J* 255(1):357–360.

10. Tanveer A *et al.* (1996) Involvement of cyclophilin D in the activation of a mitochondrial pore by Ca^{2+} and oxidant stress. *Eur J Biochem* 238(1):166–172.
11. Basso E *et al.* (2005) Properties of the permeability transition pore in mitochondria devoid of Cyclophilin D. *J Biol Chem* 280(19):18558–18561.
12. Nakagawa T *et al.* (2005) Cyclophilin D-dependent mitochondrial permeability transition regulates some necrotic but not apoptotic cell death. *Nature* 434(7033):652–658.
13. Schinzel AC *et al.* (2005) Cyclophilin D is a component of mitochondrial permeability transition and mediates neuronal cell death after focal cerebral ischemia. *Proc Natl Acad Sci U S A* 102(34):12005–12010.
14. Elrod JW, Molkentin JD (2013) Physiologic functions of cyclophilin D and the mitochondrial permeability transition pore. *Circ J* 77(5):1111–1122.
15. Rasola A, Bernardi P (2007) The mitochondrial permeability transition pore and its involvement in cell death and in disease pathogenesis. *Apoptosis* 12(5):815–833.
16. Kokoszka JE *et al.* (2004) The ADP/ATP translocator is not essential for the mitochondrial permeability transition pore. *Nature* 427(6973):461–465.
17. Baines CP, Kaiser RA, Sheiko T, Craigen WJ, Molkentin JD (2007) Voltage-dependent anion channels are dispensable for mitochondrial-dependent cell death. *Nat Cell Biol* 9(5):550–555.
18. Shanmughapriya S *et al.* (2015) SPG7 Is an Essential and Conserved Component of the Mitochondrial Permeability Transition Pore. *Mol Cell* 60(1):47–62.
19. König T *et al.* (2016) The m-AAA Protease Associated with Neurodegeneration Limits MCU Activity in Mitochondria. *Mol Cell* 64(1):148–162.
20. Giorgio V *et al.* (2013) Dimers of mitochondrial ATP synthase form the permeability transition pore. *Proc Natl Acad Sci U S A* 110(15):5887–5892.
21. Walker JE (2013) The ATP synthase: the understood, the uncertain and the unknown.

Biochem Soc Trans 41(1):1–16.

22. Bonora M *et al.* (2013) Role of the c subunit of the F_O ATP synthase in mitochondrial permeability transition. *Cell Cycle* 12(4):674–683.
23. Alavian KN *et al.* (2014) An uncoupling channel within the c-subunit ring of the F_1F_O ATP synthase is the mitochondrial permeability transition pore. *Proc Natl Acad Sci U S A* 111(29):10580–10585.
24. He J *et al.* (2017) Persistence of the mitochondrial permeability transition in the absence of subunit c of human ATP synthase. *Proc Natl Acad Sci U S A* 114(13):3409–3414.
25. Masgras I, Rasola A, Bernardi P (2012) Induction of the permeability transition pore in cells depleted of mitochondrial DNA. *Biochim Biophys Acta* 1817(10):1860–1866.
26. Zhou A *et al.* (2015) Structure and conformational states of the bovine mitochondrial ATP synthase by cryo-EM. *Elife* 4:e10180.
27. Vinothkumar KR, Montgomery MG, Liu S, Walker JE (2016) Structure of the mitochondrial ATP synthase from *Pichia angusta* determined by electron cryo-microscopy. *Proc Natl Acad Sci U S A* 113 (45):12709 –112714.
28. Hahn A *et al.* (2016) Structure of a complete ATP synthase dimer reveals the molecular basis of inner mitochondrial membrane morphology. *Mol Cell* 63(3):445–456.
29. Dickson VK, Silvester JA, Fearnley IM, Leslie AGW, Walker JE (2006) On the structure of the stator of the mitochondrial ATP synthase. *EMBO J* 25(12):2911–2918.
30. Rees DM, Leslie AGW, Walker JE (2009) The structure of the membrane extrinsic region of bovine ATP synthase. *Proc Natl Acad Sci U S A* 106(51):21597–21601.
31. Carette JE *et al.* (2011) Ebola virus entry requires the cholesterol transporter Niemann-Pick C1. *Nature* 477(7364):340–343.
32. Essletzbichler P *et al.* (2014) Megabase-scale deletion using CRISPR/Cas9 to generate a fully haploid human cell line. *Genome Res* 24(12):2059–2065.

33. Vaca Jacome AS *et al.* (2015) N-terminome analysis of the human mitochondrial proteome. *Proteomics* 15(14):2519–2524.

34. Gevaert K *et al.* (2003) Exploring proteomes and analyzing protein processing by mass spectrometric identification of sorted N-terminal peptides. *Nat Biotechnol* 21(5):566–569.

35. Watt IN, Montgomery MG, Runswick MJ, Leslie AGW, Walker JE (2010) Bioenergetic cost of making an adenosine triphosphate molecule in animal mitochondria. *Proc Natl Acad Sci U S A* 107(39):16823–16827.

36. Gomez-Fernandez JC, Harris DA (1978) A thermodynamic analysis of the interaction between the mitochondrial coupling adenosine triphosphatase and its naturally occurring inhibitor protein. *Biochem J* 176(3):967–975.

37. Wittig I *et al.* (2010) Assembly and oligomerization of human ATP synthase lacking mitochondrial subunits a and A6L. *Biochim Biophys Acta* 1797(6-7):1004–1011.

38. Gledhill JR, Montgomery MG, Leslie AGW, Walker JE (2007) How the regulatory protein, IF_1, inhibits F_1-ATPase from bovine mitochondria. *Proc Natl Acad Sci U S A* 104(40):15671–15676.

39. Bason JV, Montgomery MG, Leslie AGW, Walker JE (2014) Pathway of binding of the intrinsically disordered mitochondrial inhibitor protein to F_1-ATPase. *Proc Natl Acad Sci U S A* 111(31):11305–11310.

40. Arnold I, Pfeiffer K, Neupert W, Stuart RA, Schägger H (1998) Yeast mitochondrial F_1F_o-ATP synthase exists as a dimer: identification of three dimer-specific subunits. *EMBO J* 17(24):7170–7178.

41. Ran FA *et al.* (2013) Genome engineering using the CRISPR-Cas9 system. *Nat Protoc* 8(11):2281–2308.

42. Murphy AN, Bredesen DE, Cortopassi G, Wang E, Fiskum G (1996) Bcl-2 potentiates

the maximal calcium uptake capacity of neural cell mitochondria. *Proc Natl Acad Sci U S A* 93(18):9893–9898.

43. Clarke SJ, McStay GP, Halestrap AP (2002) Sanglifehrin A acts as a potent inhibitor of the mitochondrial permeability transition and reperfusion injury of the heart by binding to cyclophilin-D at a different site from cyclosporin A. *J Biol Chem* 277(38):34793–34799.

Figures

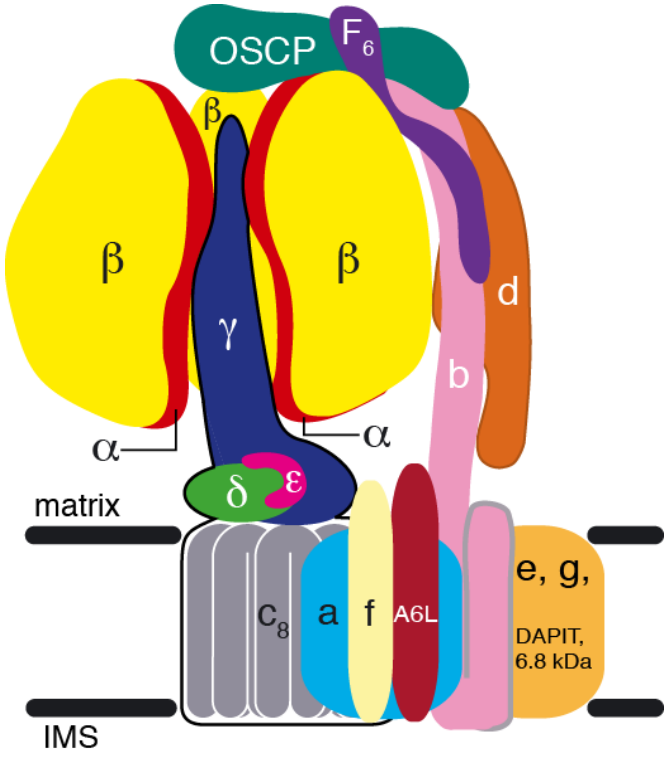

Fig. 1. Organization of subunits in one of the monomers of the dimeric ATP synthase complex in mammalian mitochondria. Black horizontal lines represent the limits of the inner membrane between the matrix and the IMS (inter-membrane space). The F_1 catalytic domain (subunit composition $\alpha_3\beta_3\gamma\delta\varepsilon$) is above; one of the α-subunits (red) has been removed to expose the γ-subunit (dark blue), lying approximately along the central axis of the spherical $\alpha_3\beta_3$ domain.

The γ-, δ- and ε-subunits are bound to the c_8-ring (grey), and together these subunits constitute the rotor. Rotation is generated by the translocation of protons through the interface between the c_8-ring and ATP6 (or subunit a; light blue). The peripheral stalk (subunits OSCP, b, d and F_6) is on the right; b has two N-terminal transmembrane α-helices. The membrane domain also contains subunits ATP8 (or A6L), e, f, g, DAPIT (diabetes associated protein in insulin sensitive tissue) and a 6.8 kDa proteolipid (6.8 kDa, or 6.8PL), each with a predicted transmembrane α-helix. The C-terminal region of ATP8, extends into the peripheral stalk; subunits ATP8 and b help keep the a-subunit in contact with the rotating c_8-ring. Subunits e, f, g, DAPIT and 6.8PL are "supernumerary" with no known roles in the generation or hydrolysis of ATP. In the dimeric complex, subunits e and g probably form the interface between monomers.

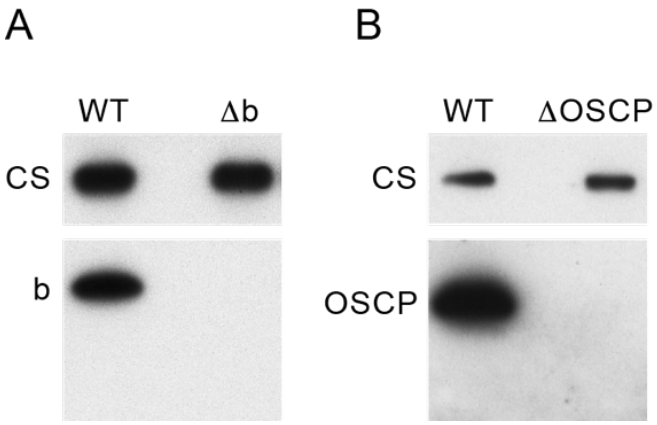

Fig. 2. Expression of the b and OSCP subunits of human ATP synthase in HAP1-WT and mutated clonal cells. (*A*) and (*B*), mitoplasts from HAP1-WT cells and from HAP1-Δb and HAP1-ΔOSCP cells, respectively, extracted with dodecylmaltoside (DDM), fractionated by SDS-PAGE and western blotted with antibodies against the corresponding subunits b and OSCP. Citrate synthase (CS) provided a loading control.

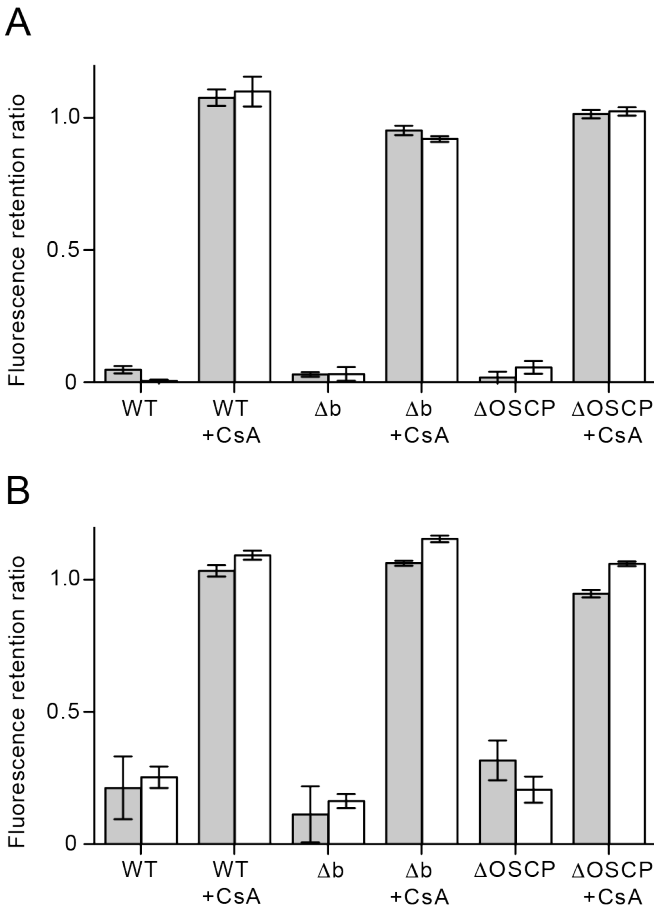

Fig. 3. The opening of the PTP in HAP1 cells. (*A*) PTP opening induced with 40 μM thapsigargin, or (*B*) with 25 μM ferutinin. HAP1-WT cells, HAP1-Δb cells and HAP1-ΔOSCP cells were stained with calcein and tetramethylrhodamine methyl ester (TMRM), and then incubated for 1 h in the presence of either thapsigargin or ferutinin. Duplicate samples were incubated first in the presence of 5 μM cyclosporin A (CsA), and then treated with either thapsigargin or ferutinin. Grey and white columns correspond to the retention ratios for calcein and TMRM, respectively, compared with cells treated with the vehicle dimethylsulfoxide only. The data are mean values ±SDs (n=4).

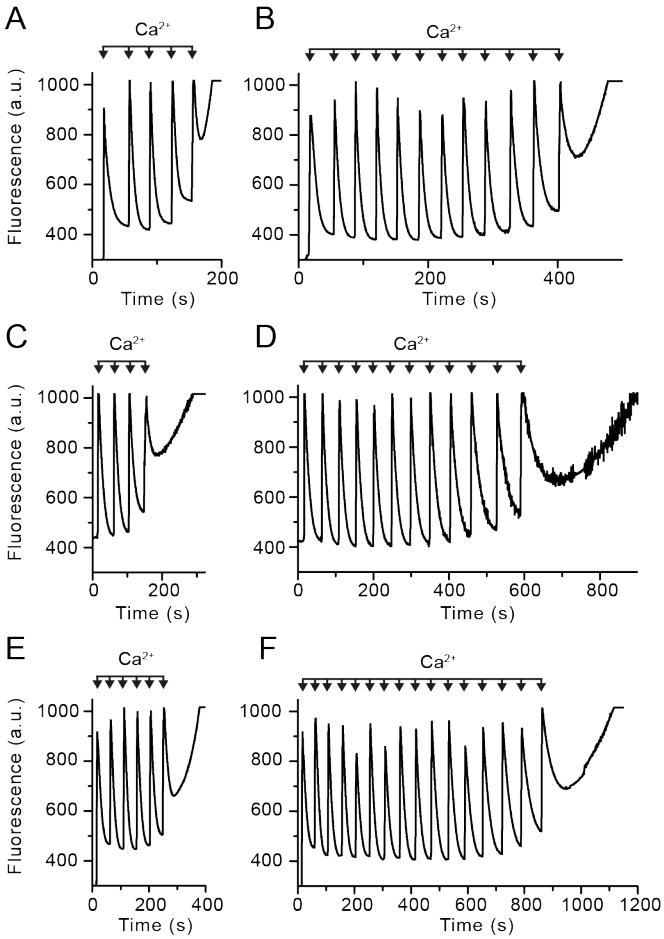

Fig. 4. Calcium induced opening of the PTP in permeabilized HAP1 cells. (*A*) and (*B*), HAP1-WT cells; (*C*) and (*D*), HAP1-Δb cells; (*E*) and (*F*), HAP1-ΔOSCP cells. The calcium retention capacity of mitochondria in digitonin permeabilized cells (20 x 10^6 cells/ml) was examined in response to pulses of 10 μM $CaCl_2$. Extra-mitochondrial Ca^{2+} was measured with Calcium green-5N fluorescence (a.u., arbitrary unit). (*A*), (*C*) and (*E*) and (*B*), (*D*) and (*F*), the calcium retention capacity in the absence and presence of cyclosporin A (1 μM), respectively.

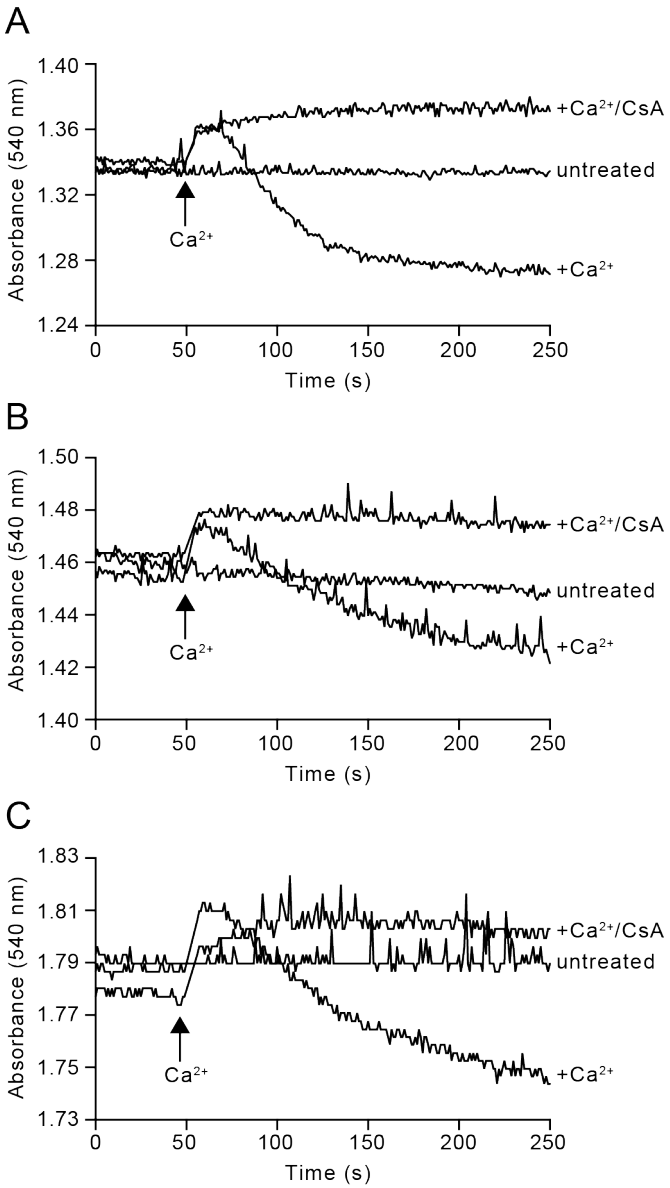

Fig. 5. Swelling of mitochondria in permeabilized HAP1 cells associated with the opening of the PTP. Swelling of 30 x 10^6 digitonin permeablized cells/ml was induced by addition of 200 µM $CaCl_2$, and monitored by the decrease in absorbance at 540 nm measured in the presence or absence of 1 µM cyclosporin A (CsA). (*A*), HAP1-WT cells; (*B*), HAP1-Δb cells; (*C*), HAP1-ΔOSCP cells.

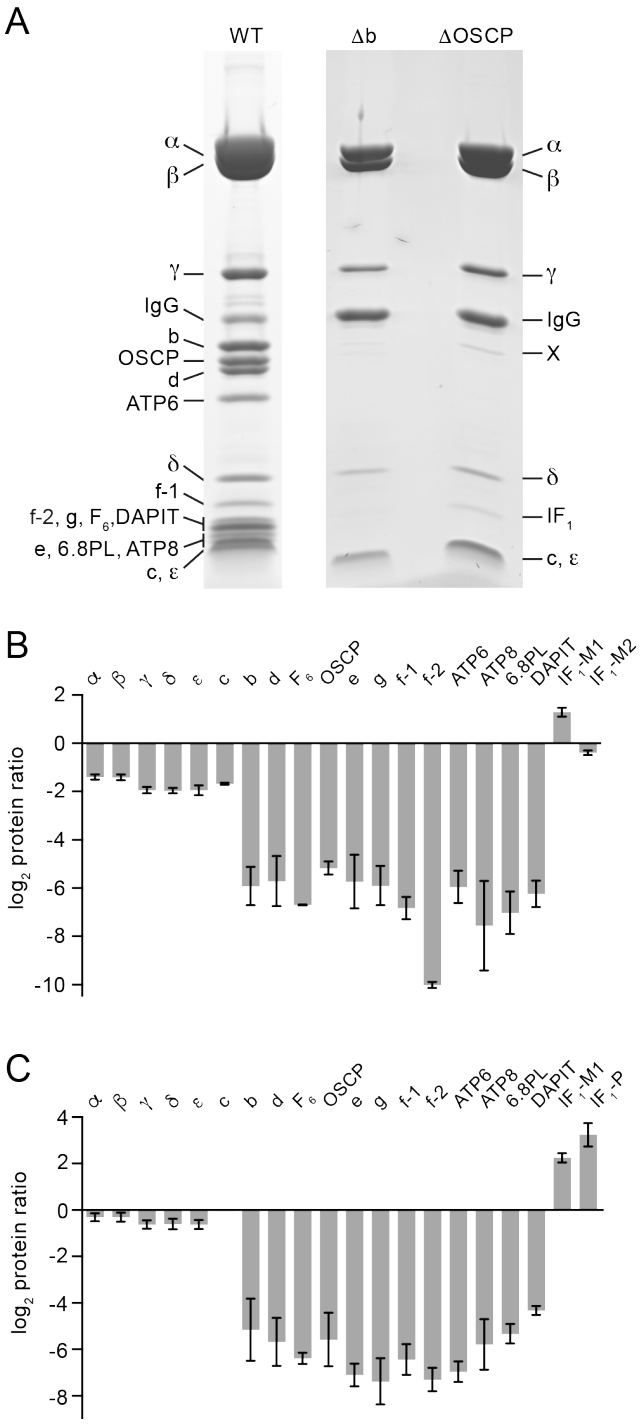

Fig. 6. Effects of the separate deletion of the b-subunit and the OSCP in HAP1 cells on the human ATP synthase complex. (*A*), Impact of removal of the b-subunit and the OSCP on the subunit compositions of the vestigial ATP synthase complexes. The complexes were purified from mitoplasts derived from HAP1-WT, HAP1-Δb and HAP1-ΔOSCP cells, and fractionated

by SDS-PAGE. Proteins were stained with Coomassie blue dye and identified by mass spectrometric analysis of tryptic digests of gel bands. In the ΔOSCP track, band X contained peptides from α- and γ-subunits, and from TMED9, PRDX3 and Rab-7a. (*B*) and (*C*), Relative abundances of subunits of ATP synthase and of forms of the ATPase inhibitor protein, IF_1 (24). The intact ATP synthase and the vestigial complexes were purified from 1:1 mixtures of SILAC-labelled cells; (*B*), HAP1-WT and HAP1-Δb cells, and (*C*), HAP1-WT and HAP1-ΔOSCP cells. Tryptic peptides were analyzed by quantitative mass spectrometry. The experiment was performed twice with reciprocal protein labelling. The bars represent median values of both relative abundance ratios determined for proteins identified in the complementary SILAC labelling experiments. Error bars show the range of the two values. In (*B*), for subunit b, peptide data assigned to the truncated form detected in HAP1-Δb cells were excluded from the calculation of the abundance ratio. In (*C*), the OSCP protein ratio for the control light/ΔOSCP heavy mixture was calculated with all available peptide values (n=174), rather than by the standard procedure, which limits the calculation to four values assigned for peptide pairs with an identified control sequence and an isotopic cluster for the ΔOSCP partner. The relative abundance of the c-subunit in HAP1-ΔOSCP samples was unchanged, with error bars smaller than the abscissa line. The histograms are derived from Fig. S4 and Datasets S1 and S2.

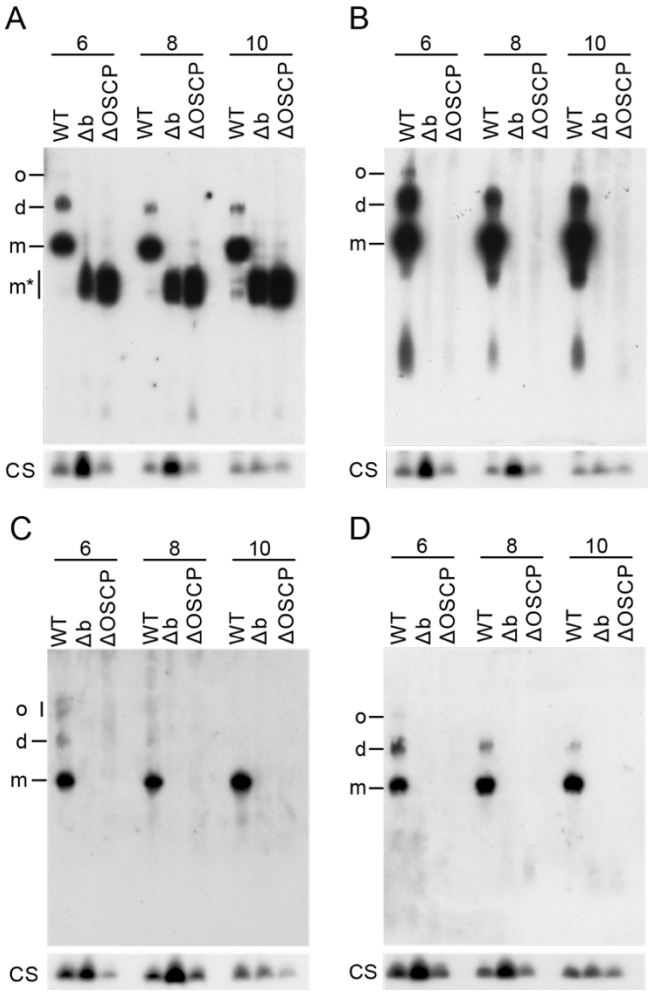

Fig. 7. Oligomeric state of ATP synthase in HAP1-WT cells, and of vestigial ATP synthase complexes in HAP1-Δb and HAP1-ΔOSCP cells. Mitoplasts from the cells were extracted with the concentrations of digitonin/protein (w/w) indicated above each lane, and fractionated by blue native-PAGE. The ATP synthase and vestigial complexes were detected by western blotting with antibodies against (*A*), the β-subunit, (*B*), the g-subunit, (*C*), the d-subunit, and (*D*), the F_6 subunit. Citrate synthase (CS) provided a loading control. o, oligomers; d, dimers; m, monomers; m*, monomeric F_1-c_8 sub-complex.

Supplementary information for:

The permeability transition in human mitochondria persists in the absence of peripheral stalk subunits of ATP synthase

Jiuya He, Joe Carroll, Shujing Ding, Ian M. Fearnley and John E. Walker

Medical Research Council Mitochondrial Biology Unit, University of Cambridge, Cambridge Biomedical Campus, Hills Road, Cambridge CB2 0XY, United Kingdom

General Methods. *ATP5F1* and *ATP5O* were disrupted in HAP1-WT cells by CRISPR-Cas9 technology (1), employing the gRNAs listed in Table S1. The HAP1-WT and clonal cells, HAP1-Δb and HAP1-ΔOSCP, were grown under standard conditions, and their growth rates were determined with an IncuCyte HD instrument. Mitoplasts were prepared from cells as described before (2, 3). Extracts of mitoplasts, made with 1% (w:v) DDM, were fractionated by SDS-PAGE, and subunits b and OSCP and citrate synthase were detected by western blotting. The oligomeric states of ATP synthase and vestigial complexes, and complexes I, II, III and IV, were examined by analysis of DDM and digitonin extracts of mitoplasts by BN-PAGE and western blotting. The ATP synthase complexes were detected with antibodies against the β-, g-, d-and F_6-subunits, and complexes I, II, III and IV with antibodies against NDUFS2, SDHA, UQCRC1, and COX4, respectively. The origins of the antibodies are given in Table S6. The oxygen consumption rates of HAP1-WT, HAP1-Δb and HAP1-ΔOSCP cells were measured in a Seahorse XFe24 instrument (3). ATP synthase was purified from mitoplasts by immuno-capture (3), and analysed by SDS-PAGE. Proteins in Coomassie blue stained bands were digested with trypsin (4) and peptides were identified by sequencing by mass spectrometry. Stable isotope labelling of proteins with amino acids in cell culture (5) (SILAC) of HAP1-WT, HAP1-Δb and HAP1-ΔOSCP cells was carried out as described before (3). After

labelling, the proteins in mitoplast samples or immuno-purified ATP synthase preparations were fractionated by SDS-PAGE, and quantitated by mass spectrometry (6). Protein ratios for the various forms of IF_1 were calculated as before (3). The protein ratios for subunit b in the samples of ATP synthase immuno-purified from SILAC labelled control and HAP1-Δb cells were re-calculated manually (median of peptide ratios) from the MaxQuant evidence file, after excluding peptide ratios assigned to a truncated form of the protein expressed in HAP1-Δb cells (see Results). The protein ratio for the OSCP in the sample of ATP synthase immuno-purified from control light/ heavy HAP1-ΔOSCP cells was re-calculated (median of peptide ratios) using all the available peptide values (n=174; $\log_2$ protein ratio -4.42) rather than the MaxQuant value ($\log_2$ protein ratio -4.37) obtained using four MULTIMSMS peptide ratios assigned for peptide pairs with a control sequence identified by MS-MS and an isotopic cluster for the ΔOSCP partner. Total RNA was purified from HAP1-Δb cells with a PureLink RNA mini kit (ThermoFisher). Any remaining traces of genomic DNA were removed by digestion with RNase-free DNase I. At the end of the digestion, DNase I was inhibited with the DNase inactivation reagent (ThermoFisher). cDNA was prepared from the RNA by reverse transcription using the RT enzyme mix and buffer from a TaqMan Gene Expression Cells-to-CT Kit (ThermoFisher). The regions of *ATP5F1* from the 40th nucleotide upstream of the ATG start codon to the junction between exons V and VI, and exons VI and VII of *ATP5F1*, respectively (Fig. S1A), were amplified with a KOD Hot Start DNA polymerase kit (Novagen) with forward primer 5' CACAGGGACGCTAAGATTG 3' paired with the reverse primer Rev1, 5' GTTTTTGCTCATTGAGTTTATC 3', or Rev2, 5' CTCCTTTTCCTGCTGTGTG 3'. The amplified fragments were purified with a gel purification kit (Qiagen) and sequenced with reverse primer Rev1 or Rev2 by Source BioScience.

Opening of the PTP. Four independent assays of PTP opening were used. In intact human cells, PTP opening was induced by thapsigargin (7), or ferutinin (8), and, in cells where the

plasma membrane had been permeabilized with digitonin, by examination of the capacity of the mitochondria to retain Ca^{2+} introduced exogenously (9) or by monitoring PTP induced swelling of mitochondria (10). The assays with thapsigargin and ferutinin, and the calcium retention assay were performed as before (3), except that, in the buffer employed in the calcium retention assay, any initial background signal was removed by incorporation of EGTA (3 μM), and changes in exogenous calcium levels were measured with 0.4 μM calcium green-5N. Pore opening was monitored also by following absorbance changes associated with the swelling of mitochondria induced by the addition of Ca^{2+} in the absence and presence of cyclosporin A. Digitonin permeabilized cells (30 x 10^6/ml) were suspended at 30°C in a buffer containing 10 mM Tris-MOPS, pH 7.4, 125 mM KCl, 1 mM KH_2PO_4, 5 mM glutamate, 2.5 mM malate and 10 μM EGTA-Tris, and stirred at 500 rpm. Calcium chloride (200 μM) was added, and the decrease in UV absorbance at 540 nm was followed. The effect of cyclosporin A on calcium induced swelling of mitochondria, was studied by adding the inhibitor (1 μM) to the permeabilised cells first, and, after 5 min, the 200 μM calcium chloride.

Table S1. Target Sites for gRNA Molecules Employed in the Disruption of Human *ATP5F1* and *ATP5O*.

gRNA	Target site
ATP5F1-1	GGGACGCTAAGATTGCTACC
ATP5F1-2	CCGCCGCCACAGCGGGTAAG
ATP5O-1	GAGAACCTAGCGGTTACGCC*
ATP5O-2	CCAGGGTGCGATGCTTCGGC

*reverse complementary sequence used as the gRNA

Table S2. Primers Employed in the Amplification by PCR of the Gene Regions Targeted by gRNAs in *ATP5F1* and *ATP5O*.

Primer	Sequence
ATP5F1-forward	CATCTTGGTCCTGCCCTGAC
ATP5F1-reverse	GCTGCAGATAGACAAGGCGA
ATP5O-forward	TACAACTCCCAGCCCGAGG
ATP5O-reverse	ACGCCAAGGTTACGGCA

A

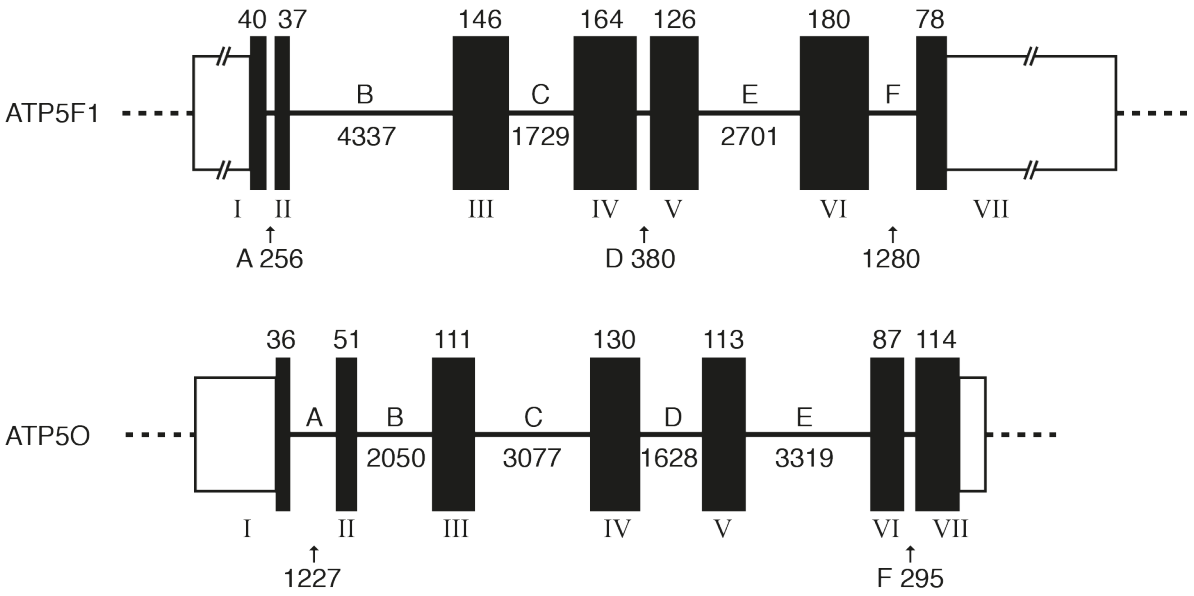

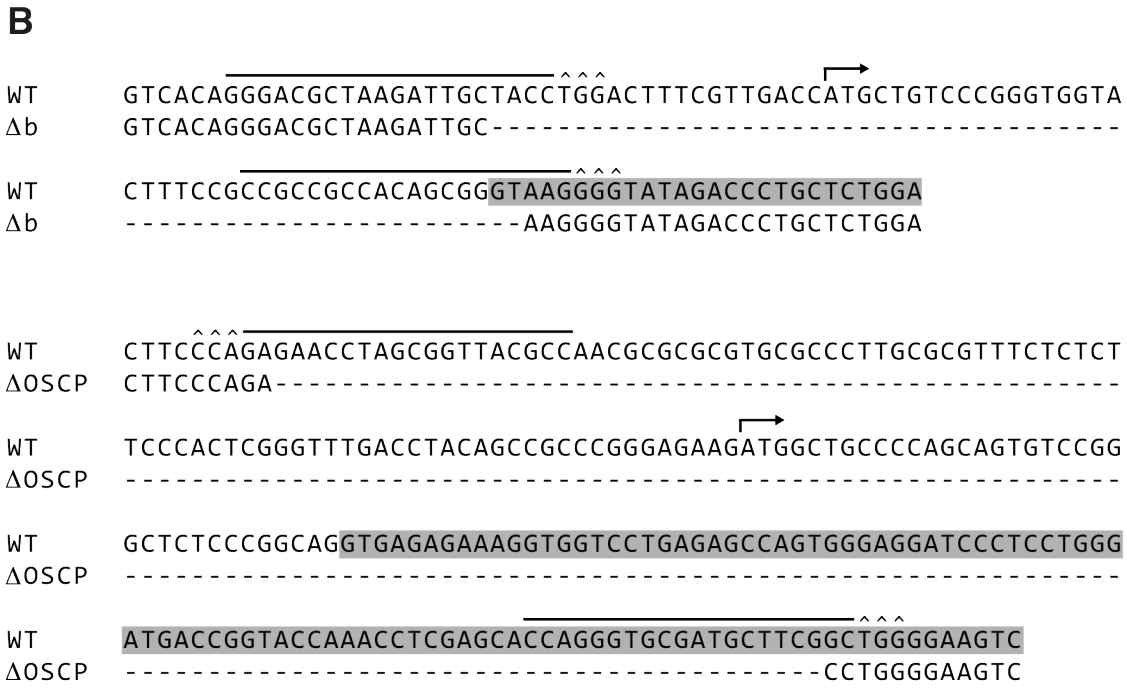

Fig. S1. Structures and disruption of *ATP5F1* and *ATP5O*. (*A*) Structures of the genes. Black and unfilled boxes represent, respectively, protein coding exons and non-coding 5'-upstream or 3'-downstream sequences within the first and last exons. Introns are depicted as continuous lines. Sizes of the exons and introns are given in base pairs. (*B*) Deletion of DNA sequences in HAP1-WT cells to produce HAP1-Δb or HAP1-ΔOSCP clonal cells. Carets indicate the PAM (protospacer adjacent motif) sequences for each guide RNA, and solid lines the guide RNA target sequences. For each gene, the upper WT sequences show part of exon I and intron A (grey box), with the arrow indicating the start codon in exon I. Dashed lines denote the deleted regions in the HAP1-Δb and HAP1-ΔOSCP cells. Both deletions remove the start codon and exon I-intron A boundaries, thereby effectively disrupting transcription and translation of the genes.

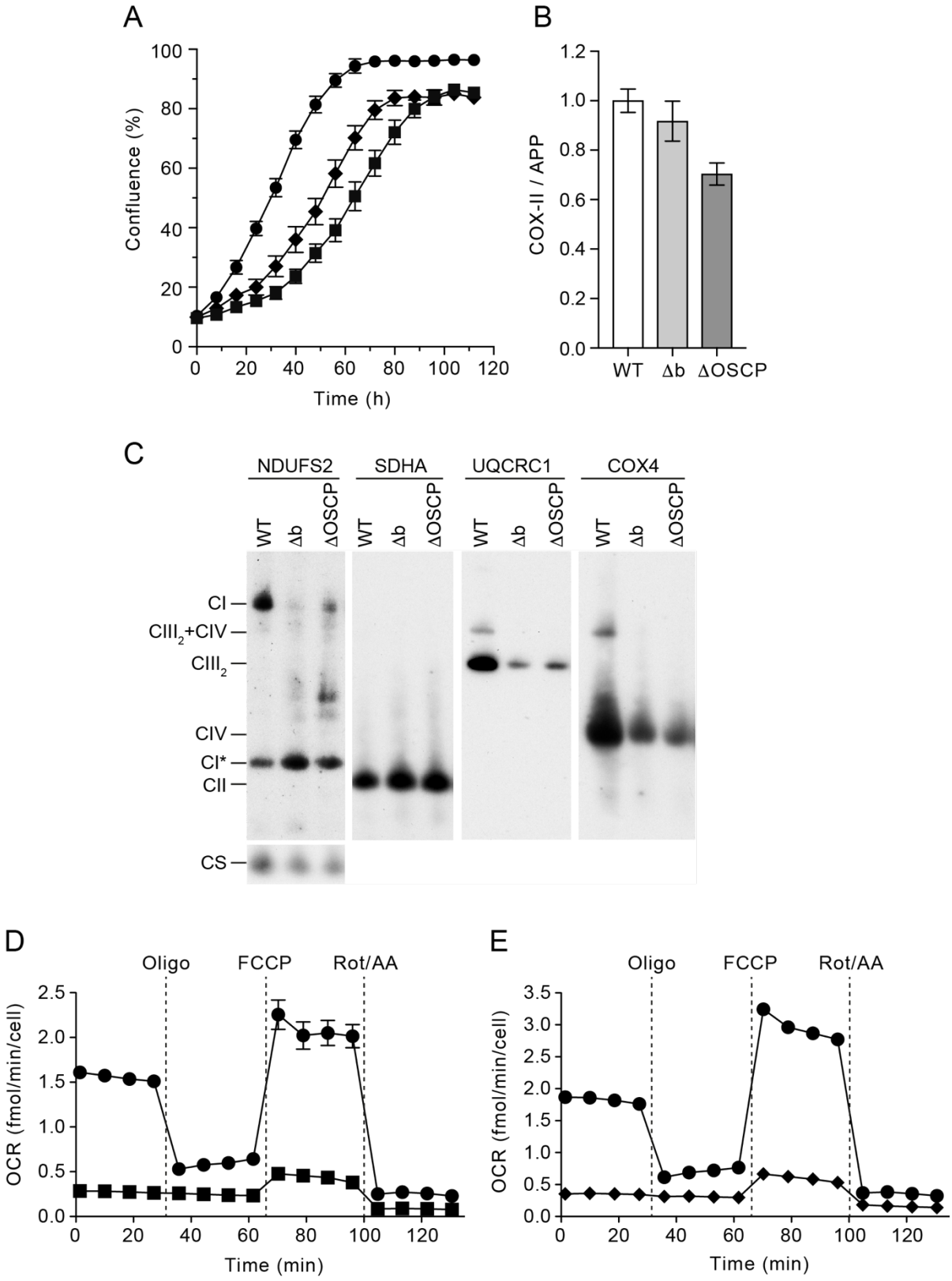

Fig. S2. Characteristics of HAP1-Δb cells and HAP1-ΔOSCP cells. (*A*) Growth rates of HAP1-WT (●), HAP1-Δb (■) and HAP1-ΔOSCP (◆) cells. About 100,000 cells were seeded into

each well of a 6-well plate, and their confluence was monitored over 120 h. Data points are the mean values ±SD (n=4). (*B*) Relative copy number of mtDNA in HAP1 cells. Regions of the genes for cytochrome oxidase subunit II (COX-II) and the amyloid precursor protein (APP) were amplified from HAP1-WT, HAP1-Δb and HAP1-ΔOSCP cells, and quantitated as indices of mitochondrial and nuclear DNA, respectively. Mean values ± SDs (n=6) are given. (*C*) Assembly of complexes I, II, III and IV in HAP1 cells. Mitoplast samples were prepared from HAP1-WT cells and HAP1-Δb and HAP1-ΔOSCP cells, extracted with DDM (3 g/g mitoplast protein), and the extracts were fractionated by BN-PAGE. Complexes were detected by western blotting with antibodies against complex I (NDUFS2), complex II (SDHA), complex III (UQCRC1) and complex IV (COX4). Citrate synthase (CS) provided a loading control. CI, complex I; $CIII_2$, complex III dimer; CIV, complex IV; $CIII_2$+CIV, complex III dimer plus complex IV; CI*, complex I sub-complex. (*D* and *E*), cellular oxygen consumption rates (OCR) of HAP1-WT (●), HAP1-Δb (■) and HAP1-ΔOSCP (◆) cells, before and after sequential addition of oligomycin (Oligo), carbonyl cyanide-4-(trifluoromethoxy)-phenylhydrazone (FCCP), and a mixture of rotenone and antimycin A (Rot/AA). Data represent the mean ±SEM (n=6-10 wells).

Table S3. Number of Calcium Pulses Recorded in Permeabilized HAP1-WT Cells.

The values in the first row refer to Fig. 4A and B. Rows 2-8 correspond to replicate experiments.

No CsA	With CsA	Ratio
5	12	2.40
6	16	2.67
3	8	2.67
11	26	2.36

6	22	3.67
7	20	2.86
7	15	2.14
4	9	2.25
Av. 6.1	Av. 16.0	Av. 2.63
SD. 2.4	SD. 6.3	SD. 0.48

Table S4. Number of Calcium Pulses Recorded in Permeabilized HAP1-Δb Cells.

The values in the first row refer to Fig. 4C and D. Rows 2-4 correspond to replicate experiments.

No CsA	With CsA	Ratio
4	12	3.00
5	13	2.60
3	7	2.33
3	6	2.00
Av. 3.8	Av. 9.5	Av. 2.48
SD. 1.0	SD. 3.5	SD. 0.42

Table S5. Number of Calcium Pulses Recorded in Permeabilized HAP1-ΔOSCP Cells.

The values in the first row refer to Fig. 4D and E. Rows 2-5 correspond to replicate experiments.

No CsA	With CsA	Ratio
6	16	2.67
7	18	2.57

4	7	1.75
3	7	2.33
3	6	2.00
3	6	2.00
Av. 4.3	Av. 10.0	Av. 2.22
SD. 1.8	SD. 5.5	SD. 0.36

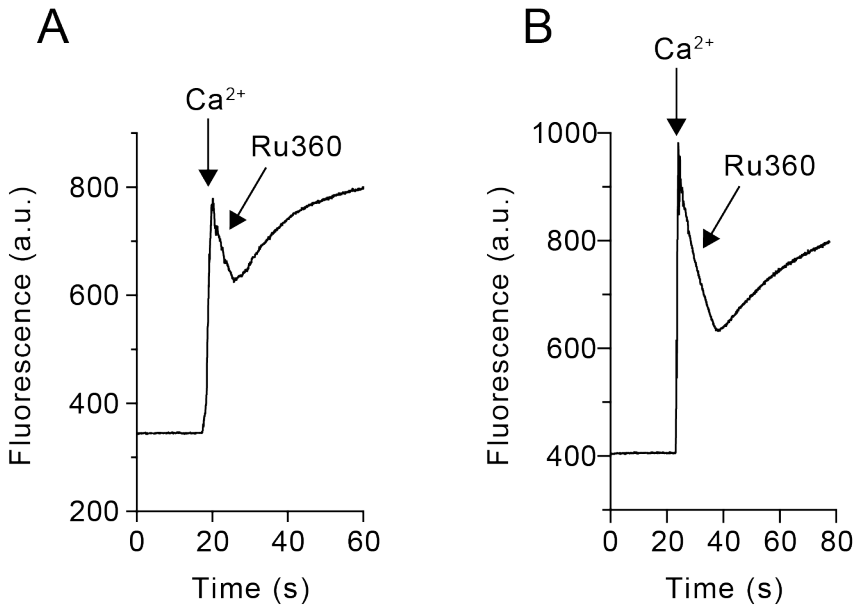

Fig. S3. Calcium uptake by HAP1 cells in the presence of Ru360, an inhibitor of the mitochondrial calcium uniporter. Digitonin permeabilized HAP1-WT cells (*A*) and HAP1-Δb cells (*B*) at 20 x 10^6 cells/ml in a KCl solution containing glutamate and malate (3), were subjected to a single pulse of 10 μM $CaCl_2$, followed by the addition of Ru360 (0.5 μM). Extramitochondrial calcium was measured with calcium green-5N fluorescence which demonstrated that Ru360 reversed the mitochondrial calcium uptake signal.

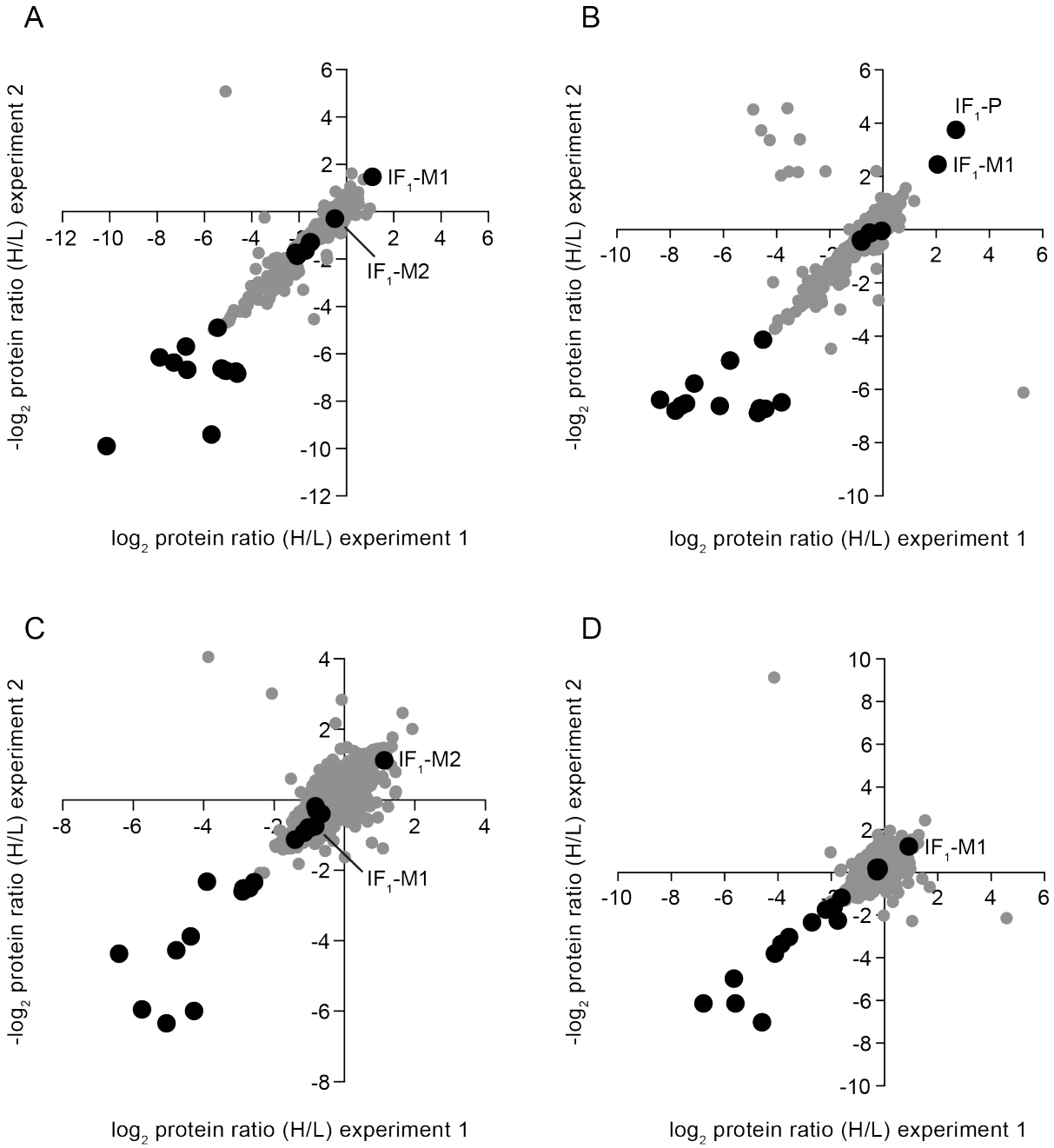

Fig. S4. Effects on protein relative abundance of the individual deletion of the b-subunit or OSCP of human ATP synthase in HAP1 cells. (*A*) and (*B*) the relative abundances of proteins in HAP1-Δb and HAP1-ΔOSCP immunopurified ATP synthase, respectively, and (*C*) and (*D*) mitoplast samples from HAP1-Δb and HAP1-ΔOSCP cells, respectively. Samples were prepared from a 1:1 mixture of HAP1-Δb or HAP1-ΔOSCP cells with HAP1-WT cells that were differentially SILAC-labelled, and the experiments were performed twice, using

reciprocal SILAC labelling orientations. The data points represent levels of all proteins where ratios were determined in both of the experimental labelling orientations. ●, ATP synthase subunits and the precursor (P), or the M1 and M2 mature forms of IF_1; ●, all other identified proteins. Protein ratios are listed in Datasets S1 to S4.

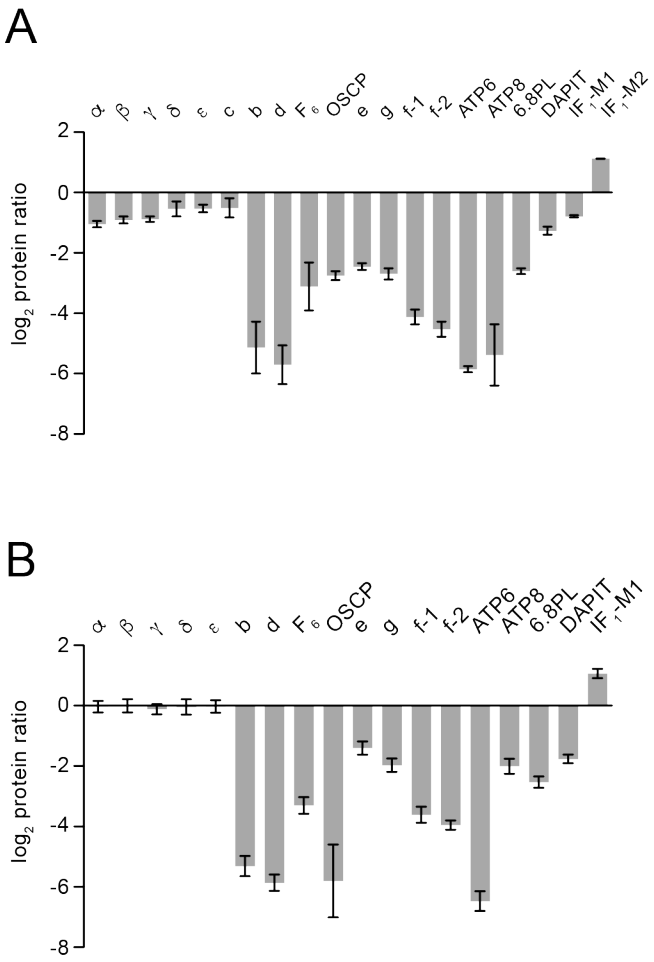

Fig. S5. Effects of the separate deletion of the b-subunit and OSCP in HAP1 cells on the levels of ATP synthase subunits in mitoplasts. (*A*) and (*B*) Relative abundance of subunits of ATP synthase and of two forms of the ATPase inhibitor protein (3). Digitonin solublilized mitoplast samples were prepared from a 1:1 mixture of SILAC-labelled HAP1-WT cells and HAP1-Δb cells (*A*), or HAP1-WT cells and HAP1-ΔOSCP cells (*B*). Proteins were separated by SDS-PAGE, stained with Coomassie blue, and gel tracks cut into equal sections. Tryptic peptides

obtained from in-gel digests were analyzed by quantitative mass spectrometry. The experiment was performed twice with reciprocal protein labelling. The bars represent median values of both relative abundance ratios determined for proteins identified in the complementary SILAC labelling experiments. Error bars show the range of the two values. The relative abundance of the c subunit in HAP1-ΔOSCP samples was not determined. The histograms are derived from the data in Fig S4 and Datasets S3 and S4.

Fig. S6. Alternative splice site between exon I and intron A formed in *ATP5F1* in HAP1-Δb cells. (*A*), The upper sequence is part of exon I and intron A (grey box) in HAP1-WT cells, with the horizontal arrow indicating the start codon in exon I. The vertical arrows show a splice site between exon I and intron A in HAP1-Δb cells (lower sequence). Dashed lines denote the deleted region in *ATP5F1* in HAP1-Δb cells. (*B*) The protein encoded from the alternative transcript in HAP1-Δb cells. The upper sequence shows the WT protein with the horizontal arrow indicating the start of the mature protein, and lower sequence the truncated protein

produced in HAP1-Δb cells. Peptides assigned to the truncated protein cover the regions within the grey boxes.

Table S6. Sources of antibodies

Protein	Source	Antibody
ATP synthase β	Santa Cruz Biotechnology	sc-33618
ATP synthase F_6	Proteintech	14114-1-AP
ATP synthase b	Santa Cruz Biotechnology	sc-514419
ATP synthase d	In-house	Rabbit antibody against recombinant bovine protein
ATP synthase g	In-house	Rabbit antibody against recombinant bovine protein
ATP synthase OSCP	In-house	Rabbit antibody against recombinant bovine protein
Citrate synthase	Proteintech	16131-1-AP
Complex I NDUFS2 subunit	Abcam	ab96160
Complex II SDHA subunit	Proteintech	14865-1-AP
Complex III UQCRC1 subunit	Sigma	HPA002815
Complex IV COX4I1 subunit	Proteintech	11242-1-AP

References

1. Ran FA *et al.* (2013) Genome engineering using the CRISPR-Cas9 system. *Nat Protoc* 8(11):2281–2308.
2. Klement P, Nijtmans LG, Van den Bogert C, Houstěk J (1995) Analysis of oxidative phosphorylation complexes in cultured human fibroblasts and amniocytes by blue-native-

electrophoresis using mitoplasts isolated with the help of digitonin. *Anal Biochem* 231(1):218–224.

3. He J *et al.* (2017) Persistence of the mitochondrial permeability transition in the absence of subunit c of human ATP synthase. *Proc Natl Acad Sci U S A* 114(13):3409–3414.
4. Wilm M *et al.* (1996) Femtomole sequencing of proteins from polyacrylamide gels by nano-electrospray mass spectrometry. *Nature* 379(6564):466–469.
5. Ong SE *et al.* (2002) Stable isotope labeling by amino acids in cell culture, SILAC, as a simple and accurate approach to expression proteomics. *Mol Cell Proteomics* 1(5):376–386.
6. Cox J, Mann M (2008) MaxQuant enables high peptide identification rates, individualized p.p.b.-range mass accuracies and proteome-wide protein quantification. *Nat Biotechnol* 26(12):1367–1372.
7. Korge P, Weiss JN (1999) Thapsigargin directly induces the mitochondrial permeability transition. *Eur J Biochem* 265(1):273–280.
8. Abramov AY, Duchen MR (2003) Actions of ionomycin, 4-BrA23187 and a novel electrogenic Ca^{2+} ionophore on mitochondria in intact cells. *Cell Calcium* 33(2):101–112.
9. Murphy AN, Bredesen DE, Cortopassi G, Wang E, Fiskum G (1996) Bcl-2 potentiates the maximal calcium uptake capacity of neural cell mitochondria. *Proc Natl Acad Sci U S A* 93(18):9893–9898.
10. Clarke SJ, McStay GP, Halestrap AP (2002) Sanglifehrin A acts as a potent inhibitor of the mitochondrial permeability transition and reperfusion injury of the heart by binding to cyclophilin-D at a different site from cyclosporin A. *J Biol Chem* 277(38):34793–34799.